Electron tunneling in azurin: the coupling across a β-sheet

JJ Regan[1], AJ Di Bilio[2], R Langen[2], LK Skov[2], JR Winkler[2], HB Gray[2*] and JN Onuchic[1*]

[1]Department of Physics, University of California at San Diego, La Jolla, CA 92093-0319, USA and [2]Beckman Institute, California Institute of Technology, Pasadena, CA 91125, USA

Background: We would like to understand how electron flow is controlled in biological molecules. Standard theories calculate the rate for long distance electron transfer (ET) as the product of electronic coupling (the square of the electron tunneling matrix element) and nuclear (Franck–Condon) factors. Much attention has been directed to the role of protein secondary and tertiary structure in the tunneling coupling, focusing on the interplay between different types of chemical bonds. Here we have evaluated the relative contributions of covalent bonds, hydrogen bonds and through-space jumps in coupling through a β-strand or across a β-sheet section of a blue copper protein, azurin.

Results: We have analyzed four distant electronic couplings in azurin. Each coupling is between the copper atom and a $Ru(bpy)_2(im)$ complex attached to a histidine on the protein surface. In three experiments the intervening medium was a simple β-strand, while in the fourth experiment it was a section of β-sheet.

Conclusions: We have shown that electron tunneling in a protein can be broken down into ET 'tubes' of pathways through specific covalent and hydrogen bonds. These ET tubes encapsulate trivial interference effects and can expose crucial inter-tube interference effects. In coupling through a β-sheet, hydrogen bonds are as important as covalent links, and are the primary source for tube interference.

Chemistry & Biology July 1995, **2**:489–496

Key words: azurin, bridge-assisted tunneling, electron transfer, pathways, tubes

Introduction

The blue copper protein azurin is important as an electron carrier in biological systems [1–4]. Based on extensive studies [5–7], it is likely that bimolecular electron transfer (ET) reactions between azurin and other redox molecules take place via His117. This residue is directly coupled to the copper atom and is close to the surface of the protein. Much less work has been done on long range ET through the protein, although Farver, Pecht and other investigators [8–11] have made an impressive start by studying ET between the copper atom and a distant disulfide bridge.

Here we address the distant coupling problem in detail. We have engineered histidine residues into azurin at positions 122, 124 and 126 along a β-strand, and have attached a $Ru(bpy)_2(im)^{2+}$ (bpy = 2,2'-bipyridine, im = imidazole) complex to the imidazole group of each of these residues [12]. These three engineered, Ru-modified proteins serve as a calibration set for analysis of ET in the $Ru(bpy)_2(im)^{2+}$ derivative of wild-type azurin, where the coupling of Ru to the Cu atom involves a section of β-sheet. The positions of the Ru complexes in the three engineered azurins as well as the modified His83 residue in the wild-type protein are shown in Figure 1. The coordinates used in the calculation of Ru–Cu couplings are based on crystal structure analyses of Nar *et al.* [4,13] and Day [14].

The multiple-site experiments have led to a new theoretical approach for ET beyond the single-pathway approach described previously [15]. In some cases, for a given donor D and acceptor A, the transfer can be thought of as 'pathway-like', wherein only a tightly grouped family of pathways (a 'tube') is relevant to the coupling. In other cases, the transfer is characterized by multiple tubes that can interfere with one another. Reducing the protein to only the relevant parts (tubes) that mediate the tunneling matrix element is a useful tool for understanding ET in a biological medium.

Results and discussion

The electron transfer model

The ET model used here arises from the standard non-adiabatic expression:

$$k_{ET} = \frac{2\pi}{\hbar} |T_{DA}|^2 F.C. \quad (1)$$

where F.C. is the Franck–Condon density of nuclear states, and T_{DA} is the tunneling matrix element:

$$T_{DA}(E_{tun}) = \sum_{d,a} \beta_{Dd} G_{da}(E_{tun}) \beta_{aA} \quad (2)$$

$$G = \frac{1}{E_{tun} - H} \quad (3)$$

In the couplings discussed here, differences in T_{DA} are expected to be much larger than differences in the $F.C.$ term, because the rates are k_{max} values with an $F.C.$ factor of order unity. Also, from experiment to experiment the local environment of D and A stays the same while the

*Corresponding authors.

 ISSN 1074-5521

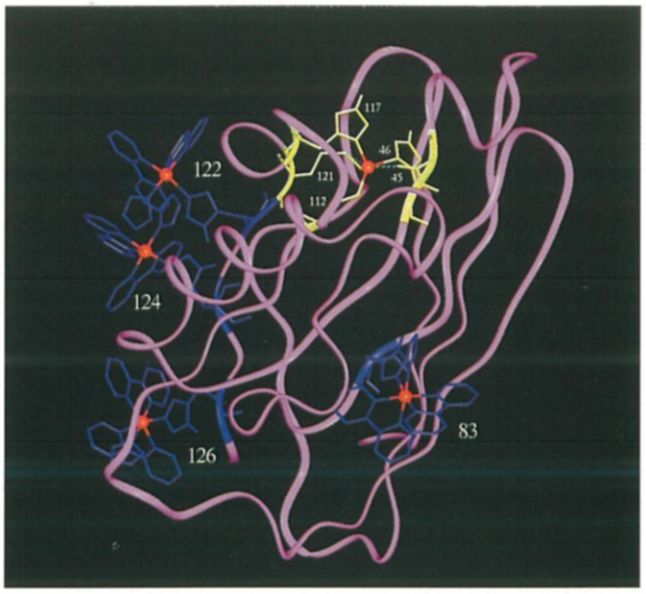

Fig. 1. A picture of the four azurin derivatives showing the copper, its ligands and the Ru(bpy)$_2$(im)(histidine) groups at positions 83,122,124 and 126. The Ru complex at position 83 points out of the page. The coordinates are derived from chain 'A', one of four azurin molecules in the unit cell of Brookhaven Protein Data Bank entry '4AZU' [4]. Molecular replacement and energy minimization were performed with Enzymix [29].

intervening medium changes. We therefore expect the relative rates to be determined by the tunneling matrix element T_{DA} alone.

All electronic properties of the protein are contained in H, a single-electron, tight-binding [16] Hamiltonian representing the protein. A 'state' in this system is an electron residing in a particular tight-binding site. The only sites used are the σ-bonding orbitals and lone-pair orbitals in the protein matrix, and two atom-centered orbitals, one at the Cu, the other at the Ru. These orbitals are simply localization sites, and are not treated in any further detail; H is just a large extended-Hückel-like matrix, with a dimension equal to the number of orbitals recognized in the protein. An off-diagonal element in H is the coupling between the two states, and is directly related to the probability that an electron will move between the two sites involved. Two of the sites in the protein are special in that they are associated with the D and A states, while the remaining states in the protein are collectively referred to as the bridge (H is partitioned into a DA subsystem and a bridge subsystem). The sum in Equation 2 is over the bridge entrance and exit states, indexed by d and a, respectively. These are the states with direct coupling to D and/or A. When the energies of D and A are close to each other, relative to their distance in energy from the closest bridge state, and when coupling to the bridge is small relative to this distance, then the DA subsystem can be viewed as an effective two-state Hamiltonian with a coupling determined by virtual occupation of the bridge [17]. The so-called tunneling energy E_{tun} is an energy parameter indicative of the energies of the D and A states (see the section entitled 'β-strand calibration of tunneling energy', below), and is expected to be the same in all experiments (because D and A are the same). All bridge states have energy zero on the energy scale used here. The direct coupling between two orbitals that share the same atom (a covalent link) is taken as a constant γ.

In this model a hydrogen bond (H-bond) is an interaction between a σ-bonding orbital (between a heavy atom and a hydrogen) and a lone-pair orbital on another heavy atom. If we arrange H so that the diagonal is ordered like the amino-acid sequence, then H-bonds (and through-space jumps) are far-off diagonal elements of H. Previous experience has shown that H-bonds are vital for mediating ET in proteins [15,18], and for strong H-bonds, such as those involved in protein secondary structure, our current results indicate that their contribution to ET is comparable to that provided by covalent links. H-bond couplings are treated as distance-independent covalent links (providing a direct coupling of γ). The Hamiltonian used here has only covalent links and H-bonds; there are no through-space jumps. Jumps do not appear to be important in the four reactions considered here, unlike the case of Ru(His72)-modified cytochrome c [18].

The important consequence of this is that the theory models the protein bridge with precisely one parameter: the ratio γ/E_{tun}. All of the covalent bonds and H-bonds in the bridge are treated as equivalent (that is, they are all γ), meaning that the Hamiltonian matrix H used with E_{tun} to compute $G = 1/(E_{tun} - H)$ is just γ times a sparse matrix of 1's. The ratio γ/E_{tun} appears in expansions of G matrix elements. This is a highly simplified picture of the protein. Despite its simplicity, the Hamiltonian used here exhibits the primary features required for this problem. There is a rough exponential decay of coupling with distance (down a tube), the coupling sign changes with each step from orbital to orbital (because $\gamma/E_{tun} < 0$ [19]), quantum interference effects (interfering tubes) arise that have a direct connection to the secondary and tertiary structure of the protein, and most importantly, the computed ratios of T_{DA} are within an order of magnitude of experimental rate ratios. More complicated Hamiltonians could and should be used but they must retain the basic features already present in our Hamiltonian (see 'β-strand calibration' section).

Tubular coupling

It is possible [20] to express the sum in Equation 2 as a sum over ET pathways in the bridge, where a pathway is a sequence of directly coupled bridge states from D to A (e.g., the $-N-C_\alpha-C-N-C_\alpha-C-$ bond sequence of a protein backbone could be a segment of a pathway). Multiple paths exist, and this leads to the notion of pathway interference. It is useful to divide interference effects into two different categories: interference within a tube and interference between tubes.

Interference within a tube, or trivial interference, arises from nearest-neighbor, next-nearest-neighbor and

backscatter effects in propagation down a simple structure, like a protein backbone, centered on a core pathway. The amide hydrogens, the lone pairs on the oxygens, even the residues themselves, all provide slightly different alternative pathways. A core pathway and its relatives, which differ only by slight nearest-neighbor deviations, are collectively called a pathway family or tube, and trivial interference is contained inside the tube. A tube is an important new concept which will help us to understand qualitatively which parts of the protein control electronic coupling. To identify a tube, we found the best pathway (the path with the largest pathway coupling magnitude [21]) between a donor and acceptor. The states in this pathway define the core of the tube. To this group of states, we added all the nearest neighboring states (those that are directly coupled to states already in the group), and then did so again. To find multiple tubes, we used a generalization of this method that differentiates between different tubes [22].

Figures 2 and 5 show the tubes selected in this way for the 126 and 83 couplings. The tubes for 122 and 124 are subsets of those seen for 126. A tube is a feature that can sometimes be blocked, or created, via molecular replacement. If T_{DA} is computed over a bridge consisting of just the sites in the pathway tubes, and if this coupling is the same as that found over the entire protein bridge, then the protein can be reduced (from an ET point of view) to just the tubes, eliminating irrelevant superstructure to expose the important structural features [20]. We now turn to a discussion of the more interesting category of interference between tubes.

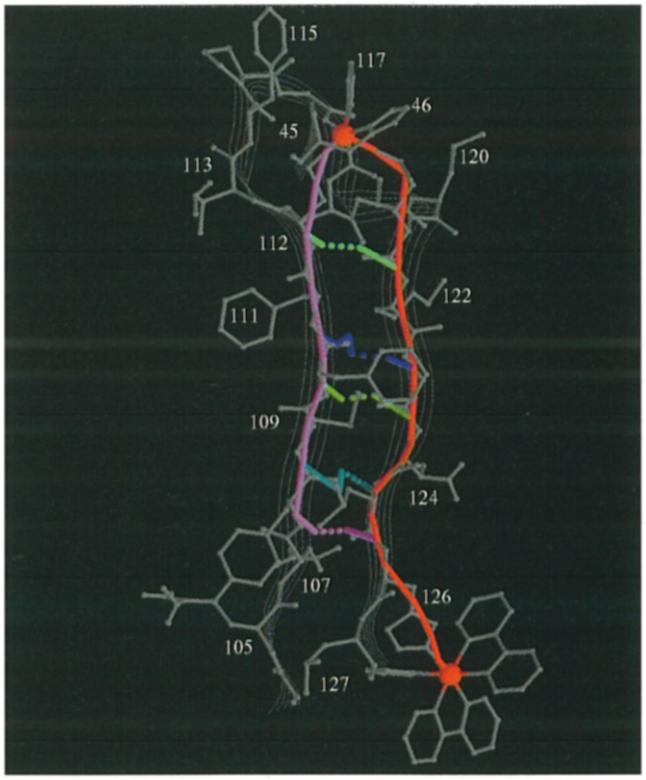

Fig. 2. Sets of pathway tubes for the ET coupling from Cu to $Ru(bpy)_2(im)$ in His126-modified azurin. The shaded lines (dashed lines are H-bonds) indicate the cores of the tubes that together are responsible for effectively all of the electronic coupling of the protein matrix. 122 and 124 are like 126, but with a subset of the tubes shown here. The coupling is dominated by the β-strand directly linked to the copper at 112.

β-Strand calibration of tunneling energy

The tunneling matrix element T_{DA} in the two-state model is a function of an energy parameter called the tunneling energy, or E_{tun}. This parameter should be indicative of the energies of the DA subsystem [17]; here it is equal to the 'band gap' (the distance from the energies of the DA subsystem to the closest eigen-energy of the bridge subsystem), since the energies of the bridge states have all been centered on zero. The value of E_{tun} is a long standing question in this model of ET. As already noted, the energy of the DA states (E_{tun}) cannot be too close to the eigen-energies of the bridge, or the effective two-state model breaks down (see above) and the electron would be delocalized over D, A and the bridge as in a metal. If it is too far away relative to γ, the contributions to the coupling from nearest-neighbor interactions and other interactions may be improperly weighted. An effective E_{tun} (to be used with our simple Hamiltonian) must be assigned to give an appropriate coupling decay down a tube (with only covalent couplings) that is consistent with experimental data. Once chosen, the same E_{tun} is used from experiment to experiment.

We emphasize here that every D–A pair is associated with a single value of E_{tun}, independent of the intervening bridge. The relevant parameter when comparing our theoretical model to experiments is γ/E_{tun}. This effective γ itself depends on E_{tun} and on the overlap between orbitals. Therefore E_{tun} is not a real physical energy since it is highly renormalized. This simple Hamiltonian, however, keeps the main feature of the wave function decay inside of the protein, that is, a single value of γ/E_{tun} is chosen to give an appropriate experimental decay with bond distance and the wave function alternates sign with every covalent bond.

To compute T_{DA}, a choice must be made for the coupling between the DA subsystem and the bridge — the various β_{Dd} and β_{aA} in Equation 2. The couplings 'weigh' the different bridge Green's function matrix elements between D and A. In our treatment of azurin in this model, there are five bridge entrances providing routes out of the donor, and one bridge exit to the acceptor. The entrances are the Cu's atomic neighbors, and the weights associated with these entrances will be labelled (as in Equation 2) β_{D46} (2.0Å), β_{D112} (2.3Å), β_{D117} (2.1Å), β_{D121} (3.2Å) and β_{D45} (2.8Å). The Cu to ligand atom distances are given in parentheses; neither residue 45 nor 121 is strictly a ligand, but each is in close proximity to the Cu atom. There is only one route into the ruthenium acceptor, namely via the X:His:NE2–Ru bond (X=83,122,124,126). Having only one bridge exit means having only one β_{aA}, which can then be pulled

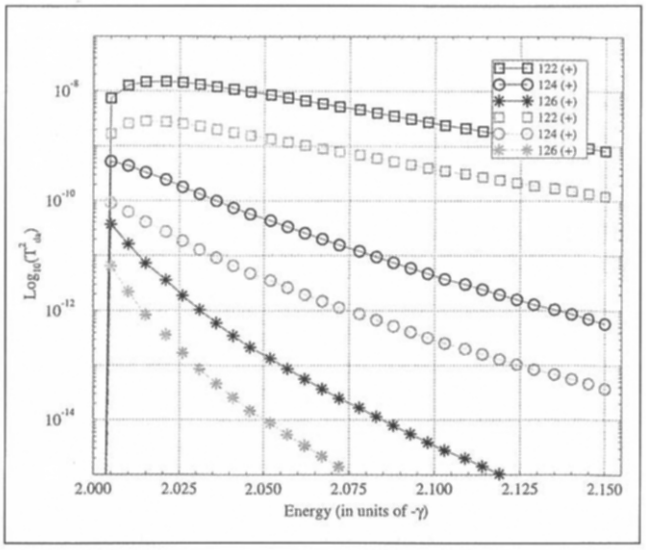

Fig. 3. T^2_{DA} (E_{tun}) versus E_{tun} (units $-\gamma$) for the 122, 124 and 126 couplings, with two different sets of weights on the donor couplings: (1) $\beta_{D112} = \beta_{D117} = \beta_{D121} = \beta_{D45} = 0.10$ (gray) and (2) $\beta_{D112} = 1.00$, $\beta_{D46} = \beta_{D117} = 0.25$, $\beta_{D121} = \beta_{D45} = 0.10$ (black).

out of the sum as a T_{DA} scaling factor that goes away in any T_{DA} ratio.

To define the effects of these parameters, two plots were made involving only the acceptors 122, 124, and 126, as these data were the easiest to interpret. A best fit to an exponential decay with *D–A* distance for these results yields a decay constant of 1.1 $Å^{-1}$ [12]; this is the softest decay that can be expected for σ-bond tunneling through a protein because a β-strand covers the longest distance with the smallest number of bonds.

Figure 3 shows a plot of T^2_{DA} as a function of E_{tun} for the 122, 124 and 126 couplings, for two different choices of weights (β). In both cases, as E_{tun} gets further from the bridge energy, T_{DA} drops off as we would expect from $G=1/(E-H)$. In this single-electron model (no shielding), G's dependence on E_{tun} may be too strong, but the general trend should be the same as expected for hole tunneling. The highest bridge eigenvalue is at 2γ ($\gamma < 0$); if we attempt to use an E_{tun} at this value or lower, we violate the two-state model. This is not a problem because, as described above, E_{tun} is chosen to provide the appropriate distance decay down a covalent chain for a given choice of *D* and *A*, and therefore it always falls outside the 'bridge band' (the range of eigenvalues of the bridge).

These weights can be given reasonable values using information available in the literature. In detailed studies of blue copper proteins, Solomon [23–25] analyzed the electronic structure of the metal and its ligands in an effort to better understand ligand-to-metal charge transfer interactions that, among other things, give these proteins their striking blue color. We only need a rough estimate of these couplings, as our model is only meant to be accurate to an order of magnitude in the bridging matrix element. Solomon found that the strongest coupling is to the SG (Cys) sulfur in residue 112, and the weakest is to the SD (Met) sulfur in residue 121. If the coupling to 112 is 1, then the coupling to 121 is roughly 0.1. Any interaction with the Gly45 carbonyl O atom is likely to be no more than the 121 coupling, so it is also set to 0.1. The coupling to the N atoms of histidine residues 46 and 117 is, on the other hand, somewhat stronger; we will take it to be about 0.25 on this scale. This ordering of Cys > His > Met will be referred to in what follows as the 'Solomon' set of weights. The 112 interaction is clearly the strongest, and will be seen to dominate the couplings in the experiments considered here, but as a rule all bridge entrances must be taken into account. Although not done here, it should be possible to position an acceptor so that Cu coupling to 112 would be unimportant compared to one of the other bridge entrances.

One set of T^2_{DA} lines (gray) in Figure 3 was generated with all weights set to 0.1, the smallest weight in the rational set. The second set of lines (black) was generated using the Solomon weights. Note that the E_{tun} dependence line for 126 (in Fig. 3) shifts up more than the line for 122 does, with this general increase in coupling weights. This is because 126 has more paths going into it from the strong 112 coupling than 122 does (Fig. 2). Because these tubes are all the same length, they interfere coherently (same sign and nearly the same magnitude), so any increase in the 112 coupling is bound to help 126 more than it will help 122. These paths traverse the ladder of H-bonds between the two adjacent β-strands seen in Figure 2. The same argument applies to 124, although the effect is not as strong since it has fewer additional paths than 126 does.

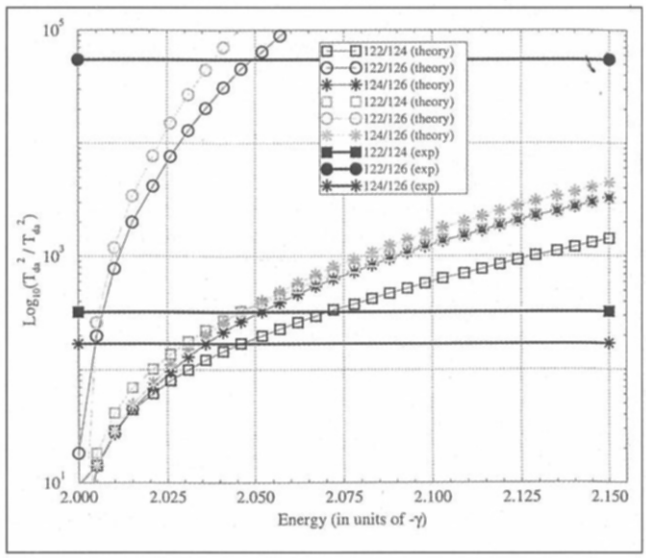

Fig. 4. Ratios of T^2_{DA} (functions of E_{tun}) compared to ratios of experimental rate constants (straight lines; see Materials and methods section). Theory lines cross experimental coupling ratio lines at roughly the same place, suggesting -2.05γ as an appropriate value for E_{tun}. Two different sets of donor couplings were used (see Fig. 3 and text). Three experimental ratios are shown even though only two ratios are uniquely determined.

Figure 4 shows how experimental data can be used to calibrate E_{tun}. In each of the ET reactions considered here, D and A (and the $F.C.$ factors) are assumed to be the same, so we expect that E_{tun} will also be the same for all reactions. But what single value of E_{tun} should be used with our highly renormalized and simplified bridge Hamiltonian? The experimental data determine it: the proper E_{tun} to use is the point where the curved theory lines intersect the straight experimental lines in this figure, $E_{tun} \sim -2.05\gamma$. Recall that E_{tun} is an effective energy parameter; this value for E_{tun} makes sense when used with the simple Hamiltonian employed in this model, and should not be converted to a real energy.

The tube results suggest that, in the cases of 122, 124 and 126, the principal coupling is provided by the tubes from 112 and to a much lesser extent 121 (because of weaker copper coupling), and that in any event, these tubes interfere coherently. Because of the dominance of the 112 tubes, ratios of T_{DA} values (for acceptors on the same β-strand) will not depend on the choice of weights so strongly that shifting the weights slightly will select a substantially different E_{tun}. For the case with all weights the same, the dominant tube leaves the Cu at 121 to feed directly into 122, and so on. For the Solomon set of weights, the main coupling is through 112. Since the paths down the 112 strand are just a constant three steps longer than those down the 121 strand, the ratios in one strand are similar to those in the other, so both sets of theory lines in Figure 4 (for each set of weights) cross experimental lines at roughly the same energy.

As Figure 3 shows, the Solomon weights shift 126 up more than 124, which itself shifts up more than 122, and this causes both the ratios 124/126 and 122/124 to drop (Fig. 4). Unfortunately, the 122/124 ratio drops more than the 124/126 ratio, because 124 is helped more relative to 122 than 126 is helped relative to 124. Thus, the theoretical 124/126 ratio stays higher than the theoretical 122/124 ratio, in contrast to the experimental results. This minor discrepancy is a result of the the rough treatment of H-bonds in this model — they are all treated in exactly the same way. The actual N–O bond length of the 112–121 H-bond feeding 122 is 0.2–0.3Å longer than the ones feeding 124 and 126, and the coupling to 122 should not improve as much as it does when the 112 weight is increased. If the lengths of these H-bonds were incorporated into the model, it would resolve this problem. However, a detailed description of the tuning of H-bonds is not the aim of this paper; rather, we seek a qualitative bridge model with only one adjustable parameter.

Table 1. Matrix elements for bridge entrance and exit points.

d	X=122	X=124	X=126
112:Cys:SG–Cu	–6.1e-05	–5.3e-06	–3.1e-07
121:Met:SD	–3.1e-04	–1.4e-05	–6.6e-07
117:His:ND1–Cu	–3.0e-06	–1.5e-07	–7.0e-09
46:His:ND1–Cu	1.1e-06	7.9e-08	4.4e-09
45:Gly:O	2.1e-06	1.5e-07	7.8e-09
112:Cys:SG–Cu	6.3e-05	5.5e-06	3.3e-07
121:Met:SD	–3.2e-04	–1.4e-05	–7.0e-07
117:His:ND1–Cu	–3.0e-06	–1.6e-07	–7.4e-09
46:His:ND1–Cu	1.1e-06	7.2e-08	3.5e-09
45:Gly:O	2.2e-06	1.4e-07	6.8e-09

G_{da} (-2.05γ) (units $-\gamma^{-1}$), a = X:His:NE2-Ru for the full protein (top half) and the subset (bottom half) of the protein relevant to the β-strand experiments (shown in Fig. 2). The agreement between these two sets of results shows that the rest of the protein can be neglected in the coupling calculations.

Table 2. Ratios of best tubes G'_{da} to full G_{da} for bridge entrances 112 and 121 ($E_{tun} = -2.05\gamma$).

Entrance	122	124	126
112	5.1	4.2	5.2
121	1.8	3.4	5.3

Tubes versus full protein

The full G_{da} matrix elements taken between bridge entrance and exit points for the full protein bridge are provided for $E_{tun} = -2.05\gamma$ in the upper half of Table 1. From this table, and the expression for T_{DA} in Equation 2, we can immediately see which bridge entrances are important in which reactions, and the effects of the β weights, since the weights multiply these numbers directly in the T_{DA} sum. The largest bridge couplings to the β-strand acceptors (122, 124, 126) are, of course, via 112 and 121 (though the stronger 112:SG–Cu coupling will make the tubes involving residue 112 far more important).

From Table 1, the total bridge coupling from the bridge entrance at 112 to the exit at 126 is 3.1×10^{-7}. If G_{da} is computed over just the orbitals in the 112→126 β-strand tubes, each tube offers a coupling of about -1.6×10^{-6}, a factor of 5.2 better. This comparison of β-strand tubes to the full protein G_{da} matrix elements for the bridge entrances 112 and 121 (with a common exit at the Ru) is set out in Table 2. The tubes always do better than the full protein (for the same entrance and exit), and sometimes they do much better.

Two effects are important here. The first effect is called trivial interference, and it acts to make the best tube to full protein ratios larger. Any time a bridge is simply expanded, without any significant changes like the introduction of new routes between the D and A, the extra side trips on the paths destructively interfere with the couplings and energies of the states on the important paths, reducing the overall coupling between any two points. The numbers in the lower half of Table 1, representing G_{da} elements taken over a 30 % subset of the protein (just the combination of what is shown in Figs 2 and 5), are slightly larger than those for the entire protein in the upper half, all by roughly the same constant factor (around 1.05). The full protein

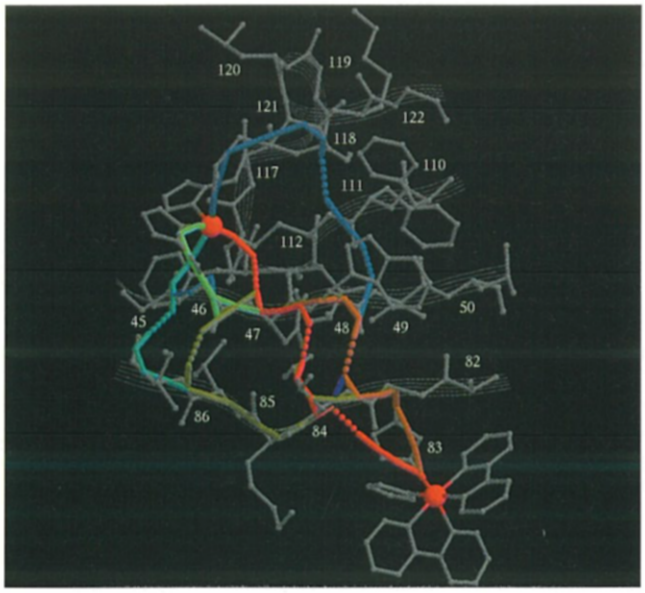

Fig. 5. Sets of pathway tubes for the ET coupling from Cu to Ru(bpy)$_2$(im)(His83) in wild-type azurin. For residue 83, multiple tubes traverse a β-sheet between donor and acceptor.

coupling between two points will generally be smaller than that provided by a single tube. Moreover, the longer the distance covered by the tube (the more 'surface area' it has), the more it will be dragged down by this effect — which is why the ratios in Table 2 generally increase with *DA* separation (note the 122, 124, 126 sequence from 121).

The second important effect is the interference that results from multiple tubes. If multiple tubes interfere constructively, this will increase the full protein number relative to the single best tube number, decreasing the best tube to full protein ratio (and of course the opposite will happen for destructively interfering tubes). There are multiple constructively interfering tubes from 112 to 126, and these increase the full protein number to keep this ratio as low as 5.2, lower than the 5.3 ratio for the shorter, more direct route via residue 121.

Before moving on to discuss the coupling to residue 83, we emphasize the main points of the discussion of the β-strand calibration. (1) The weights to use on the copper should obey Cys > His > Met, with a reasonable set given by $\beta_{D112} = 1.00$, $\beta_{D46} = \beta_{D117} = 0.25$, $\beta_{D121} = \beta_{D45} = 0.10$. (2) The measured rates for 122, 124 and 126 make sense within the model, and the effects of constructive tube interference can already be seen for residues 126 and 124. (3) These same experimental results suggest that a reasonable E_{tun} to use is -2.05γ. (4) The coupling provided by the β-strand tubes is reduced when the full protein is included, due to trivial interference, and the longer the tube, the more the coupling is diminished by this effect.

The coupling to residue 83

Coupling to residue 83 is expected to be difficult to understand, because the direct line from the Cu to the Ru site is perpendicular to the intervening backbone structure; there is no simple path as there is in each of the cases considered above. In the coupling of the Cu to the Ru at 83, not only do multiple tubes cross each other, but multiple tubes take different exits from the copper (Fig. 5).

The best tube to 83 leaves the copper via 112. The tube takes an H-bond (112:Cys:SG → 47:Asn:N–HN) to get to 47, avoiding the long detour through the length of 46. It then takes an H-bond 48:Trp:N–HN → 84:Thr:OG1 (the second best path takes the H-bond connecting 48:Trp:O → 84:Thr:N–HN) to get to the 80's section of the chain, to finally enter the His residue at 83, and thus reach the Ru complex. Additional tubes are made possible by an H-bond connecting the 120's chain to the 110's chain (121:Met:O → 112:Cys:N), and a second H-bond connecting the 110's chain to the 40's chain (111:Phe:O → 49:Val:N–HN). If we neglect everything in the protein except for the sites in this best tube, the resulting G_{da} (d=112:SG–Cu) is 7.8×10^{-5}. If only this tube's contribution were included in the plots of T^2_{DA} in Figure 4, its contribution would cross the experimental lines at -2.05γ, in agreement with the 122, 124 and 126 calibration.

Significance

One goal of ET theories is the prediction of tunneling couplings in proteins. Our current work provides a new framework to explore and understand the features of the protein structure that mediate such couplings.

We have shown that a protein, as represented by its atomic coordinates, can be converted to a very simple Hamiltonian which has just enough information to retain all essential features of the electron tunneling problem. The coupling derived from this model can be broken down into contributions from individual tubes, each of which is a family of similar pathways through specific sequences of covalent bonds and H-bonds. The tubes encapsulate trivial interference effects and can expose crucial inter-tube interferences. The set of all tubes that are important to the coupling can be identified — and the rest of the protein can be neglected. A purely quantum mechanical effect like tube interference is directly related to the secondary and tertiary structure of the protein. H-bonds are central in this effect, as they are the primary factor distinguishing a protein from what would otherwise be an effective (and uninteresting) one-dimensional chain. The step from a tube analysis of a protein to experimental design is obvious, as there will be situations where a tube can be created or blocked by an appropriate mutation.

We have applied the tube approach to interpret four couplings in azurin. By analyzing ET that

proceeds through more than a single strand, we have been able to show the crucial role that H-bonds have in the coupling across a β-sheet. In addition, we have begun to investigate how the couplings between copper and its different ligands may influence the directionality of long range ET.

Materials and methods

Recombinant wild-type *Pseudomonas aeruginosa* azurin [26] was modified according to the following procedure: pure azurin (A_{628}/A_{280} 0.60–0.62) was equilibrated with aqueous sodium carbonate (300 mM, pH 8.5) and the concentration of protein adjusted to 0.1–0.2 mM. An equivalent amount of $[Ru(bpy)_2CO_3]\cdot 4H_2O$ [27] (freshly prepared in 300 mM sodium carbonate, λ_{max} 510 nm; ϵ 9200 $M^{-1}cm^{-1}$) was added and the reaction mixture titrated to pH 7.2–7.6 with dilute hydrochloric acid. The reaction was allowed to take place for 12 h in a capped vial at room temperature. $Ru(bpy)_2(H_2O)$ (His83)azurin (λ_{max} (Ru) 488 nm; >90 % yield) was isolated by means of cation exchange chromatography (FPLC, Mono S) using a gradient of sodium acetate buffer (25–300 mM; pH 4.5). Small variations of the reaction conditions did not affect the yield of azurin modified at His83. The aquo complex was equilibrated with a solution containing 500 mM imidazole•HCl, 100 mM NaCl, and 10 mM $CuSO_4$ (pH 7.5) for four days at room temperature. The product, $Ru(bpy)_2(im)$ (His83)azurin (λ_{max} (Ru) 491 nm, 436nm (sh)), was stored at 4° C in the same imidazole-containing buffer (and repurified before use in kinetics experiments). The Cu^+ to Ru^{3+} rate constant was determined by a standard flash/quench method [28]:

$$Cu^+Ru^{2+} \xrightarrow{h\nu} Cu^+[Ru^{2+}]^* \quad (4)$$

$$Cu^+[Ru^{2+}]^* + [Ru(NH_3)_6]^{3+} \rightarrow Cu^+Ru^{3+} + [Ru(NH_3)_6]^{2+} \quad (5)$$

$$Cu^+Ru^{3+} \rightarrow Cu^{2+}Ru^{2+} \quad (6)$$

$$Cu^{2+}Ru^{2+} + [Ru(NH_3)_6]^{2+} \rightarrow Cu^+Ru^{2+} + [Ru(NH_3)_6]^{3+} \quad (7)$$

Transient absorption measurements (reduced Ru-azurin 20mM; $[Ru(NH_3)_6]Cl_3$ 8–12 mM; μ = 0.1 phosphate buffer pH 7.0; 25° C) gave a rate constant of 1.1(1) x 10^6 s^{-1} for Equation 6. After 480 nm excitation (1.0–1.5 mJ pulse, 25 ns pulse width), electron transfer was monitored at 632.8 nm (CW HeNe laser) for $Cu^{+/2+}$ and 430 nm (arc lamp) for $Ru^{3+/2+}$. Analysis of analogous flash/quench experiments on $Ru(bpy)_2(im)$ (HisX) azurin (X=122,124,126) derivatives yielded the following rate constants for Equation 6: 122, 7.1(4) x 10^6 s^{-1}; 124, 2.2(2) x 10^4 s^{-1}; 126, 1.3(6) x 10^2 s^{-1} [12]. For electron transfer from Cu^+ to all four Ru^{3+} sites (83,122,124,126), activationless rates are estimated to be within 5 % of observed rates ($-\Delta G° = 0.75$eV; $\lambda \approx 0.8$ eV) [12].

Theoretical calculations were performed with the greenpath program [22]. Tube visualization was done using RasMol v2.5 (R. Sayle (1994), Greenford, Middlesex, UK) as modified by F.K. Chang.

Acknowledgements: We thank David Beratan and Spiros Skourtis for many helpful comments. Mike Day kindly provided the coordinates of the $Ru(bpy)_2(im)$ (His83)azurin structure. We thank F.K. Chang for help with tube visualization. Research at Caltech was supported by the NIH (DK19038). Research in San Diego was supported by the NSF (grant MCB-93-16186). J.J.R. was also supported by the Berkeley Program in Mathematics in Biology (NSF grant DMS-94-06348).

References

1. Adman, E.T. & Jensen, L.H. (1981). Structural features of azurin at 2.7Å resolution. *Isr. J. Chem.* **21**, 8–120.
2. Gray, H.B. (1986). Long range electron transfer in blue copper proteins. *Chem. Soc. Rev.* **15**, 17–30.
3. Sykes, A.G. (1991). Active-site properties of the blue copper proteins. *Adv. Inorg. Chem.* **36**, 377–408.
4. Nar, H., Messerschmidt, A., Huber, R., Van de Kamp, M. & Canters, G.W. (1991). X-ray crystal structure of the two site-specific mutants his35gln and his35leu of azurin from *Pseudomonas aeruginosa*. *J. Mol. Biol.* **218**, 427–447.
5. Van de Kamp, M., Floris, R., Hall, F.C. & Canters, G.W. (1990). Site-directed mutagenesis reveals that the hydrophobic patch of azurin mediates electron transfer. *J. Am. Chem. Soc.* **112**, 907–908.
6. Van de Kamp, M., Silvestrini, M.C., Brunori, M., Beeumen, J.van, Hall, F.C. & Canters, G.W. (1990). Involvement of the hydrophobic patch of azurin in the electron-transfer reactions with cytochrome c551 and nitrite reductase. *Eur. J. Biochem.* **194**, 109–118.
7. Mikkelsen, K.V., Skov, L.K., Nar, H. & Farver, O. (1993). Electron self-exchange in azurin: Calculation of the superexchange electron tunneling rate. *Proc. Natl. Acad. Sci. USA* **90**, 5443–5445.
8. Farver, O. & Pecht, I. (1992). Long range intramolecular electron transfer in azurins. *J. Am. Chem. Soc.* **114**, 5764–5767.
9. Farver, O., Skov, L.K., Nar, H., Van de Kamp, M., Canters, G.W. & Pecht, I. (1992). The effect of driving force on intramolecular electron transfer in proteins — studies on single-site mutated azurins. *Eur. J. Biochem.* **210**, 399–403.
10. Farver, O., *et al.*, & Pecht, I. (1993). Intramolecular electron transfer in single site mutated azurins. *Biochemistry* **32**, 7317–7322.
11. Broo, A. & Larsson, S. (1991). Electron transfer in azurin and the role of aromatic side groups of the protein. *J. Phys. Chem.* **95**, 4925–4928.
12. Langen, R., Chang, I.J., Germanas, J.R., Richards, J.H., Winkler, J.R. & Gray, H.B. (1995). Electron tunneling in proteins: Coupling through a β-strand. *Science.* **268**, 1733–1735.
13. Nar, H., Messerschmidt, A., Huber, R., Van de Kamp, M. & Canters, G.W. (1991). Crystal structure analysis of oxidized *Pseudomonas aeruginosa* azurin at pH 5.5 and pH 9.0 — a pH-induced conformational transition involves a peptide bond flip. *J. Mol. Biol.* **221**, 765–772.
14. Day, M.W. (1995). X-ray crystallographic studies on electron transfer proteins. PhD thesis, California Institute of Technology.
15. Beratan, D.N., Onuchic, J.N., Winkler, J.R. & Gray, H.B. (1992). Electron-tunneling pathways in proteins. *Science* **258**, 1740–1741.
16. Ashcroft, N.W. & Mermin, N.D. (1976). *Solid State Physics.* W.B. Saunders, New York.
17. Skourtis, S.S. & Onuchic, J.N. (1993). Effective 2-state systems in bridge-mediated electron transfer — a green's function analysis. *Chem. Phys. Lett.* **209**, 171–177.
18. Wuttke, D.S., Bjerrum, M.J., Winkler, J.R. & Gray, H.B. (1992). Electron-tunneling pathways in cytochrome *c*. *Science* **256**, 1007–1009.
19. Beratan, D.N. (1986). Electron tunneling through rigid molecular bridges: Bicyclo[2.2.2]octane. *J. Am. Chem. Soc.* **108**, 4321–4326.
20. Regan, J.J., Risser, S.M., Beratan, D.N. & Onuchic, J.N. (1993). Protein electron transport: Single versus multiple pathways. *J. Phys. Chem.* **97**, 13083–13088.
21. Onuchic, J.N., Andrade, P.C.P. & Beratan, D.N. (1991). Electron tunneling pathways in proteins: A method to compute tunneling matrix elements in very large systems. *J. Chem. Phys.* **95**, 1131.
22. Regan, J.J. (1995). Electron tunneling in proteins: the electron tunneling matrix element. PhD thesis, University of California at San Diego.
23. Lowery, M.D. & Solomon, E.I. (1992). Axial ligand bonding in blue copper proteins. *Inorg. Chim. Acta* **200**, 233–243.
24. Solomon, E.I., Baldwin, M.J. & Lowery, M.D. (1992) Electronic structures of active sites in copper proteins: Contributions to reactivity. *Chem. Rev.* **92**, 521–542.
25. Solomon, E.I. & Lowery, M.D. (1993). Electronic structure contri-

butions to function in bioinorganic chemistry. *Science* **259**, 1575–1581.
26. Chang, T.K., *et al.*, & Richards, J.H. (1991). Gene synthesis, expression, and mutagenesis of the blue copper proteins azurin and plastocyanin. *Proc. Natl. Acad. Sci. USA* **88**, 1325–1329.
27. Kimura, T., Sakurai, T., Shima, M., Nagai, T., Mizumachi, K. & Ishimori, T. (1982). The structure of carbonatobis(2,2'-bipyridine)Ru(II)tetrahydrate. *Acta Cryst. B* **38**, 112–115.
28. Chang, I.J., Gray, H.B. & Winkler, J.R. (1991). High driving force electron transfer in metalloproteins — intramolecular oxidation of ferrocytochrome c by $Ru(2,2'\text{-bpy})_2(im)(His\text{-}33)^{3+}$. *J. Am. Chem. Soc.* **113**, 7056–7057.
29. Lee, F.S., Chu, Z.T. & Warshel, A. (1993). Microscopic and semimicroscopic calculations of electrostatic energies in proteins by the polaris and enzymix programs. *J. Comput. Chem.* **14**, 161–185.

Received: **26 Jun 1995**; revisions requested: **7 Jul 1995**; revisions received: **10 Jul 1995**. Accepted: **10 Jul 1995**.